Theoretical Investigations into the Structural and Electronic Influences on the Hydrogen Bonding in Doped Polyaniline

ARTICLE *in* SYNTHETIC METALS · APRIL 2003

Impact Factor: 2.25 · DOI: 10.1021/jp030398w

2 AUTHORS, INCLUDING:

Andy Monkman
Durham University
416 PUBLICATIONS **9,835** CITATIONS

SEE PROFILE

Theoretical Investigations into the Structural and Electronic Influences on the Hydrogen Bonding in Doped Polyaniline

Joel P. Foreman* and Andrew P. Monkman

Organic Electroactive Materials Research Group, Department of Physics, University of Durham, Durham DH13LE, U.K.

Received: March 31, 2003; In Final Form: June 13, 2003

DFT-based electronic structure calculations are performed on a series of compounds designed to model the hydrogen bonding present in sulfonic acid-doped polyaniline. A thorough investigation of the structural and electronic influences on the hydrogen bonding at the B3LYP/6-311++G(2d,2p) level reveals a number of previously unknown features of such systems. Rearrangements of both the geometry and electronic configuration indicate that the creation of a hydrogen bond between the N−H group in the polyaniline models and the O−S group in the sulfonic acid models increases the ability of the phenyl−nitrogen backbone to transfer electron density.

1. Introduction

The interest shown in polyaniline (PANi) as a synthetic, conducting polymer has continued to grow in recent years.[1] This is partly due to its high chemical and environmental stability, but also it is simple and cheap to process, and its salts exhibit levels of electrical conductivity approaching that of metals. The structure of polyaniline has been well documented[2] and in its emeraldine base form (EB; Figure 1) consists of a series of Ph−N repeat units, where the nitrogen exists in either an imine or amine environment. EB is electrically insulating due to an empty conduction band, but doping with a strong acid protonates both iminic nitrogens to give emeraldine salt (ES; Figure 1). ES is electrically conducting by virtue of its half-filled polaron band, and this has led to a variety of potential applications.[3]

While EB is reasonably soluble in standard hydrogen-bonding solvents, ES is less so, and this leads to problems with processability. However, if bulky sulfonic acids are used as the dopant for ES, solubility levels are much higher.[4] In particular, PANi doped with (±)-10-camphorsulfonic acid (CSA) in *m*-cresol (MC) shows great promise with a variety of metallic properties having been observed. Of note is the electrical conductivity of PANi/CSA/MC films, which can reach 10^3 S cm^{-1}, comparing very favorably with that of copper (10^5 S cm^{-1}). This system forms a so-called "synergistic triad", where the properties of the films created from solution depend critically on the presence of all three components. It is assumed that the triad is arranged so that sulfonic acid groups on CSA hydrogen bond to the PANi N−H groups.[5]

There is a wealth of experimental data available on the structure and uses of polyaniline and its derivatives. However, it is only recently that theoretical methods have begun to address the geometry and electronic structure of such polymer/dopant compounds. To the best of our knowledge the main hydrogen bond between the N−H in PANi and the S═O in CSA has not been modeled using ab initio methods before, though semiempirical calculations on a similar system exist.[6] These indicate that sulfate anions (SO_4^{2-} or HSO_4^-) prefer to interact with the radical cationic form of oligomeric PANi in a face-on fashion with one of the phenyl rings. In contrast, the semiempirical models proposed by Ikkala et al.[5] have methanesulfonic acid and tosylenesulfonic acid anions interacting end-on with oligomeric PANi. The authors suggest that a form of "molecular recognition" exists in the system analogous to that observed in biochemistry. Their model shows MC cyclically associating with the PANi/CSA with specific structural requirements such as the presence of a phenyl ring and hydrogen bond donor or a critical distance between the hydrogen-bonding site and the van der Waals-bonding site.

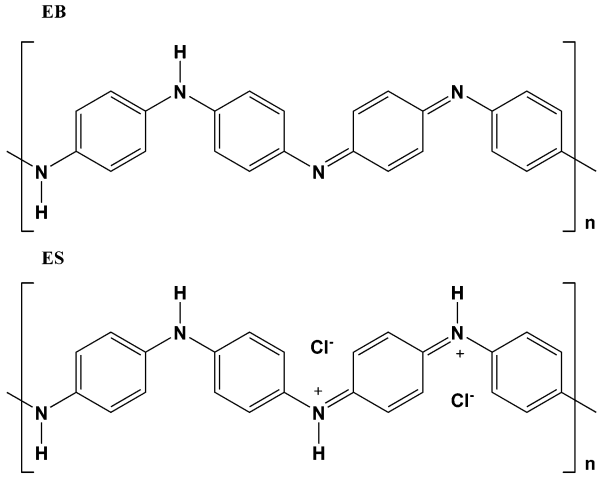

Figure 1. Structures for EB and ES.

In fact, the use of theoretical methods to investigate the structure and energetics of various aspects of polyaniline and its derivatives has mostly concentrated on semiempirical techniques. In particular, hydrogen bonding between water and PANi oligomers has been investigated using both the EHMO-CO[7] and CNDO/AM1[8] methods. These results suggest the conductivity improves upon formation of hydrogen bonding between water or *m*-cresol and PANi though the origins of this effect are not entirely clear. Also, an AM1 study on the interactions between poly(bisphenol A carbonate) and PANi monomers, dimers, and trimers[9] suggests that hydrogen bonding

* To whom correspondence should be addressed. E-mail: joel.foreman@dur.ac.uk.

10.1021/jp030398w CCC: $25.00
Published on Web 08/30/2003

does occur in longer polymer chains. A number of other semiempirical papers exist on various aspects of PANi. These include grafting of polymers to enhance properties,[10] conformational analysis and UV−vis spectra,[11] structure and energetics of PANi polarons and bipolarons,[12] adsorption onto metal surfaces,[13] and finally substitution effects in diphenylamine.[14]

Examples of the application of ab initio and hybrid DFT methods to polyaniline and its derivatives are rarer. Calculations necessarily on the smallest oligomeric forms of PANi at the HF level with small basis sets[15] agree with the half-filled polaron band model. Additionally, several papers exist on a variety of features of aniline trimers at the higher B3LYP and CIS levels[16] where the main conclusions suggest that the use of small subunits of PANi to model gross properties is valid. Theoretical modeling of these subunits (e.g., small aromatic amines) is a nontrivial exercise. Previous studies indicate that double-ζ basis sets with polarization functions are the absolute minimum for accurately modeling aromatic amines.[17] In comparison, the structures of aromatic phosphines are relatively accurately modeled by ab initio methods with double-ζ basis sets.[18] However, the inclusion of electron correlation is required for the precise calculation of energies and quantities obtained directly from the wave function (e.g., atomic properties).[19] More recently, a number of papers have applied hybrid DFT methods to aniline oligomers and conclude that these methods are suitable for modeling such compounds.[20] In fact, the use of hybrid DFT methods to investigate the general nature of hydrogen bonding in a variety of systems has become much more common.[21]

A partial crystal structure of oligomeric PANi doped with CSA obtained locally indicates that the sulfonic acid repeatedly bridges two adjacent PANi chains, locking them together with hydrogen bonding. With the gross structural aspects of the system known, it is now possible to model the hydrogen bonding in greater detail with a view to explaining its influence on the conductivity of the system. In this paper we detail computational efforts to model the geometry and electronic structure of the hydrogen bonding in doped PANi.

2. Methods

Complexes between PANi and CSA contain too many atoms to be effectively modeled by DFT at present. To address this issue, we have chosen a series of smaller model compounds intended to represent the most important functional groups and interactions present in the structure. In ES, two distinct canonical nitrogen environments exist, an amine and an iminium cation. The actual nitrogen environment in ES will of course vary between these two extremes, and the perfect model would be an average of the two. An average model of this kind is untenable; hence, both nitrogen environments are modeled where possible. The amine nitrogen is modeled by dimethylamine, Me_2NH (DMA), diphenylamine, Ph_2NH (DPA), [1,5]diazocane (DAZO), and 6,12-diaza-1,5,7,11(1,3)-tetrabenzenacyclododecaphane (DTC), while the iminium cation nitrogen is modeled by the methylmethyleneamine cation, $CH_3NH{=}CH_2$ (MMA), and the (4-iminocyclohexa-2,5-dienylidene)phenylamine cation (ICPA). The full chemical structures can be seen in Figure 2, where it becomes clear which models most closely resemble PANi. The simpler models are included to obtain a limited statistical spread for this hydrogen bond type and not to provide absolute values. Clearly, DTC is the best PANi model used in this work, and results using this model should be most comparable to experimental findings. DTC itself is two diphenylamine molecules arranged face-on (cf. PANi) bridged underneath by two propyl groups. CSA is modeled using the methanesulfonic acid anion, $CH_3SO_3^-$, (MSA) and DMSO, and with the former bridging DTC across its two amine groups, an effective model for PANi/CSA is obtained (DTC−MSA). The propyl bridges are an essential part of the model that effectively lock the system together and prevent the diphenylamine groups from drifting apart during optimization. In this conformation, the rings will be slightly hindered from adopting a more twisted conformation. However, this has the same effect as the packing forces that reduce ring twisting in the crystal structure. In addition, from the crystal structure we know that PANi chains are bridged on both sides by CSA, so each propyl group also acts as a dummy CSA on the opposite side of the PANi chain.

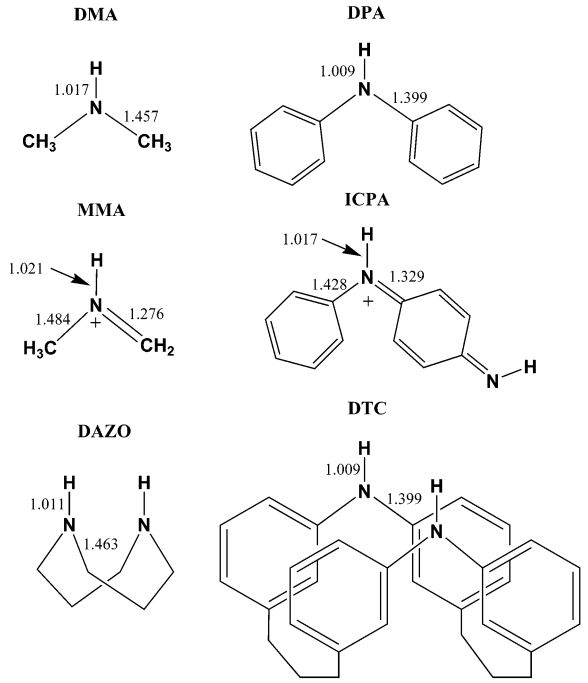

Figure 2. B3LYP/6-31G(d,p)-optimized structures for the six monomers used in the project. Selected bond lengths are included (Å).

Last, as the focus of this paper is the N−H···O−S hydrogen bond, several potentially interesting structural features of the PANi/CSA/MC triad are not dealt with and will be addressed in later papers. These include the role the solvent (MC) and the extra CSA carbonyl group play (either can hydrogen bond to PANi or CSA) and the influence of phenyl−phenyl interactions.[22]

Eight complexes consisting of a hydrogen bond donor and a hydrogen bond acceptor were created (Figure 3) and fully optimized using the B3LYP exchange-correlation functional[23] with the 6-31G(d,p) basis sets.[24] Symmetry conditions were imposed where appropriate to reduce the number of unique integrations necessary and reduce the time taken for jobs to complete. C_s symmetry was applied to DMA, MMA, DMSO, DMA−MSA, DMA−DMSO, MMA−DMSO, and DAZO−MSA, C_{2v} to DAZO, C_2 to DTC, C_3 to MSA, and C_1 to everything else. Harmonic frequency calculations are also performed at this level to give bond stretching frequencies (reported unscaled) and zero-point energy (ZPE) corrections. Basis set superposition error (BSSE) in the dimers is accounted for using the counterpoise method[25] at the higher B3LYP/6-311++G(2d,2p) level.[26] All calculations are performed using Gaussian 98[27] on Compaq Alpha machines.

The first of two analyses used to describe the electronic structure of the system is Weinhold's natural bond orbital (NBO) theory.[28] This is based on a method that transforms the electronic

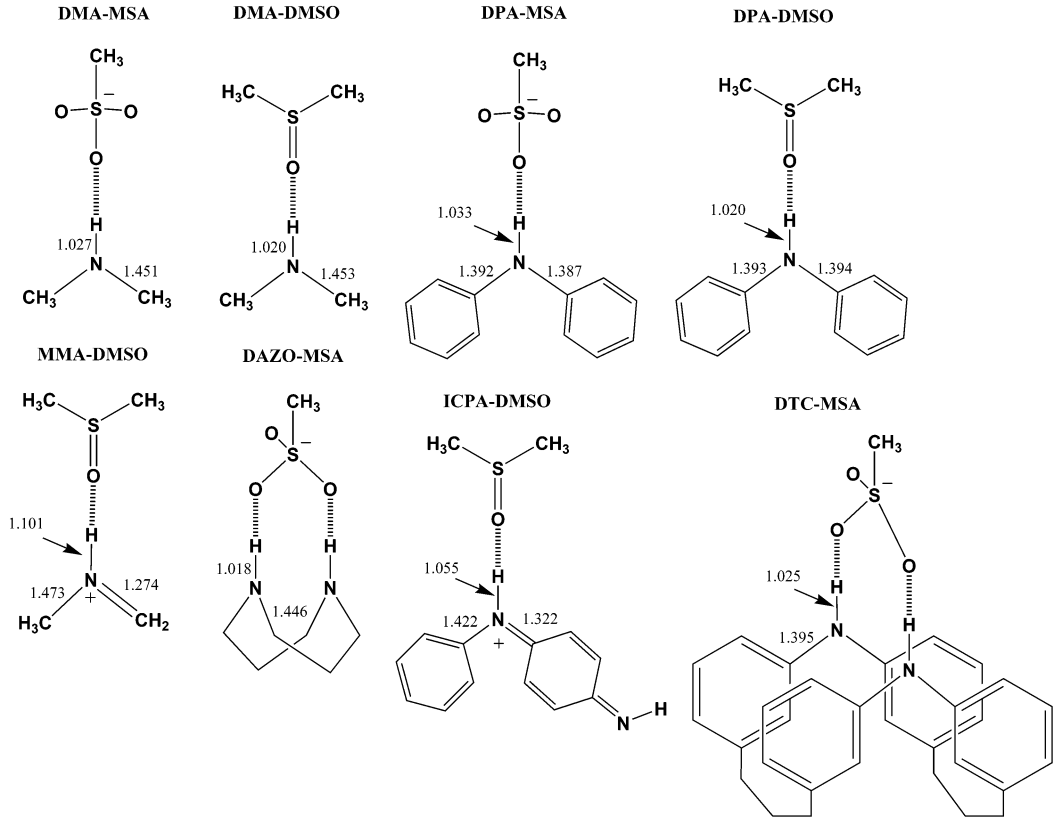

Figure 3. B3LYP/6-31G(d,p)-optimized structures for the eight dimers created in the project. Selected bond lengths are included (Å).

wave function into a set of orthonormal one- and two-center localized "natural orbitals" that correspond to the traditional chemist's notion of Lewis orbitals. The set of doubly occupied natural orbitals faithfully recreates the standard Lewis picture of bonding, each one- or two-center orbital representing a lone pair or bond, respectively. Departures from this ideal picture result in sparsely occupied non-Lewis orbitals, such as antibonding orbitals and Rydberg orbitals, which act as electron sinks. All possible interactions between the Lewis and non-Lewis orbitals are assessed, and the electron transfer is estimated using second-order perturbation theory and measured by the stabilization energy, $E^{(2)}$. In addition, natural population analysis sums the occupancies of each natural atomic orbital to give an atomic population, *N*. NBO analyses of the B3LYP/6-311++G-(2d,2p) wave function were performed using NBO 5.0.[29]

The electronic structure is further analyzed using Bader's atom-in-molecules (AIM) theory,[30] which assigns chemical meaning to the total electronic charge density, ρ, and its derivative, $\nabla\rho$, by means of the electronic wave function. Atomic subsystems are defined from the molecular density using a series of boundary surfaces with zero flux in $\nabla\rho$. The atomic population is calculated by integration of the density over this "atom". The standard classification of critical points in ρ is (n, m), where n is the number of nonzero eigenvalues at the critical point and m is the sum of signs of the eigenvalues. In this particular work, bond critical points (the (3, −1) critical points that occur at the point of zero gradient between bonded atoms) are analyzed as they contain the most useful information about the bonding in a system. The ellipticity, ϵ, of the bond is a measure of the ratio of the two negative eigenvalues at its bond critical point. Values vary from 0.0 for pure single bonds (σ-type) to approximately 0.4 for π-type bonds and provide a potentially useful measure of the aromaticity of bonds adjacent to delocalized phenyl systems. The value of ρ at the bond critical point (ρ_c) also provides useful information about the degree of ionic/covalent character in a bond. Larger values of ρ_c tend to correspond to covalent bonds where there is more density between the atoms, and vice versa for ionic bonds. In addition, other types of bonding can be revealed by these values (e.g., hydrogen bonds and "intermediate interactions"). Topological analyses of the B3LYP/6-311++G(2d,2p) wave function were performed using EXT94B and PROAIMV, both part of Bader's AIMPAC[31] suite of programs.

3. Results

(a) Structures (Table 1). The crystal structure of oligomeric PANi/CSA/MC mentioned earlier suffered from disorder, mostly in solving the location of the MC molecules. However, the gross structural features of the system can clearly be observed and also the geometry of the hydrogen bonds. A more complete theoretical examination of the oligomer structure will be published at a later date, but for current comparison purposes the experimental geometry is as follows. The hydrogen bond length, r(HB), hydrogen bond angle, a(HB), and HNCC dihedral angle, d(HNCC), are 1.988 ± 0.045 Å, 167 ± 3°, and 37 ± 6°, respectively.

The theoretical hydrogen bond geometry of DTC−MSA (Table 1) compares very well with experiment, as it is the dimer that most closely resembles doped oligomeric PANi. Nonetheless, the optimized dihedral angles show one phenyl ring on each nitrogen settling near the experimental value, with the other significantly more planar. The mean of all four dihedrals is ∼16° lower than the experimental orientation due to the fact that, without a more complete structure, the phenyl rings have more freedom to adopt a more preferred conformation. The presence of more PANi oligomers, longer oligomers, larger dopant models, and solvent models averages out the localized geometry effects observed here.[22] However, DTC−MSA remains the optimum model in this work, and as the calculated hydrogen

TABLE 1: B3LYP/6-31G(d,p)-Optimized Structural Properties[a]

dimer	r(HB)	ω(HB)	a(HB)	d(HNCC)	Δr(N−H)	$\Delta\omega$(N−H)	Δr(O−S)	$\Delta\omega$(O−S)	Δr(N−C)	$\Delta\omega$(N−C)	$\Delta\lvert d$(HNCC)$\rvert$	E_{HB}
DMA−MSA	1.939	322	160.4		+0.010	−137	+0.011	0, −28	−0.006	−40, −12		27.3
DMA−DMSO	2.076	95	165.3		+0.003	−43	+0.008	−23	−0.004	+31, +8		8.5
MMA−DMSO	1.463	462	165.3		+0.080	−1290	+0.042	−139	−0.011, −0.002	+36, +25		125.0
DAZO−MSA	1.975	107, 106	160.0		+0.007	−97, −104	+0.006	+3, −36	−0.017	+84, +193		23.1
DPA−MSA	1.797	320	168.2	22.4, 13.7	+0.024	−413	+0.018	−1, −54	−0.012, -0.007	+14, +45	-8.1	69.5
DPA−DMSO	1.937	370	166.6	25.6, 14.8	+0.011	−193	+0.016	−42	−0.006, -0.005	+5, +31	−3.8	18.4
ICPA−DMSO	1.633	149	169.4	6.2, 40.5	+0.038	−684	+0.033	−133	−0.006, −0.007	+14, −39	−0.6	90.0
DTC−MSA	1.921, 1.925	117, 106	165.7, 166.7	6.5, 38.8, 2.8, 34.9	+0.016	−253, −268	+0.007, +0.012	+1, +2	−0.003, −0.005	+5, −2	+4.4, −3.2	38.5

[a] Bond lengths r in Å, vibrational frequencies ω in cm^{-1}, bond angles and dihedral angles a and d in deg, and hydrogen bond strengths E_{HB} in kJ mol^{-1}. The table is divided into alkyl-based models followed by aryl-based models. Δ values refer to the change in property on complexation. Where appropriate (a) symmetric stretches are followed by antisymmetric stretches, (b) two instances of one bond type are both reported, (c) the mean bond strength is reported for dimers with two hydrogen bonds, and (d) single bonds are followed by double bonds.

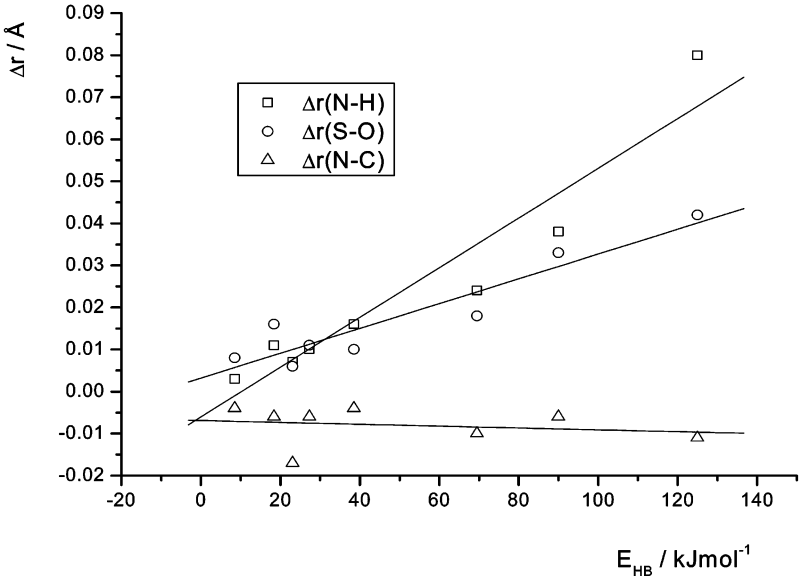

Figure 4. Graph showing the correlation between the changes in bond length on dimerization (Δr) and the hydrogen bond strength (E_{HB}).

bond geometries of the other seven models clearly show they are less suitable for direct comparison with experiment, they will be used for observing trends.

The key bond lengths and angles of the optimized dimers are shown in Figure 3. With one or two exceptions, most of these values lie within the accepted ranges for their bond types. The N−C bond lengths in DTC−MSA are shorter than the expected ∼1.45 Å. This is also the case for the N−C bond in both DPA complexes and is a strong indication that the N−C bond in these complexes is intermediate between single and double (σ and π). The N−C and N═C bond lengths in ICPA−DMSO are in the usual range, and the HNCC dihedral angles are split as observed previously for DTC−MSA. However, in this case, the split is caused by the double bond restricting rotation about the N═C bond. Interestingly, the N−C bonds are very similar in length in DTC−MSA (1.390−1.397 Å), and yet the dihedral split is still observed. Two very short hydrogen bond lengths occur in both MMA−DMSO and ICPA−DMSO, where an extra interaction appears to exist between the S═O and N═C bonds. Accordingly, less significance is applied to further results from these two complexes.

An important part of this section is comparing the geometry of the dimers with that of their constituent monomers to assess what structural effect the creation of a hydrogen bond between them has. It is known from previous studies that the effect is relatively small,[32] and that is borne out here, where Δr is always <0.1 Å. Both r(N−H) and r(O−S) decrease on dimerization as electron density is removed to create the adjacent hydrogen bond. In fact, the reduction in r(N−H) and r(O−S) is proportional to the hydrogen bond strength (Figure 4). Next, r(N−C) consistently decreases on complexation, and while it is possible that this is another cause for the lengthening of the adjacent N−H bond through removal of electron density, it is more likely that there is another reason for this effect. This is supported by the less obvious broad correlation between Δr(N−C) and the bond strength (Figure 4). More likely this effect is directly caused by a change in the electronic nature of the Ph−N system on creation of the hydrogen bond. As expected, most changes in bond stretching frequency mirror changes in bond length. However, one anticipated trend that failed to emerge was a correlation between the hydrogen bond length and its stretching frequency. The usefulness of a scale, where potentially easily obtained experimental bond stretching frequencies would correspond to predicted bond strengths, was not underestimated. Unfortunately, the relatively weak nature of the bonds involved produced no observable trends.

The change in the sum of the HNCC dihedral angles, $\Delta|d$(HNCC)|, effectively measures the change in the interplanar angle between two neighboring phenyl rings on creation of the hydrogen bond. The values for both DPA complexes are negative, indicating an increase in the planarity of the Ph−N−Ph backbone on dimerization. The value for ICPA−MSA is small because ICPA is already close to its optimum configuration before dimerization. The N═C section is almost planar,

TABLE 2: B3LYP/6-311++G(2d,2p)//BLYP/6-31G(d,p) NBO Properties[a]

dimer	ΔN_C	ΔN_N	ΔN_H	ΔN_O	ΔN_S	ΔN_{LP}, ΔE_{LP}	$\Delta E^{(2)}_{LP(N)\rightarrow C=C^*}$	$\Delta E^{(2)}_{C=C\rightarrow C=C^*}$	$\sum E^{(2)}_{LP(O)\rightarrow N-H^*}$
DMA−MSA	−0.008	+0.044	−0.073	+0.022	−0.005	−0.014, +0.13910			40.5
DMA−DMSO	−0.007	+0.006	−0.041	−0.004	−0.011	−0.010, +0.03542			24.2
MMA−DMSO	−0.002, +0.044	+0.023	−0.031	+0.043	+0.002				276.0
DAZO−MSA	−0.010	+0.044	−0.082	+0.004	−0.003	−0.043, +0.17790			32.7
DPA−MSA	−0.015	+0.020	−0.069	+0.024	−0.008	−0.065, +0.13102	+46.3	−2.3	81.7
DPA−DMSO	−0.007	+0.022	−0.045	+0.023	−0.001	−0.033, +0.02425	+24.5	−0.9	48.1
ICPA−DMSO	−0.022, +0.004	+0.020	−0.049	+0.062	−0.006			+0.0	152.2
DTC−MSA	−0.040, −0.039	+0.039, +0.037	−0.061, −0.061	+0.008, +0.010	−0.007	−0.038, −0.042, +0.11735, +0.11639	+15.9, +18.6	+0.0, +0.0	48.5, 48.1

[a] Natural populations N in e and second-order delocalization energies $E^{(2)}$ in kJ mol^{-1}. The table is divided into alkyl-based models followed by aryl-based models. Δ values refer to the change in property on complexation. Where appropriate (a) two instances of one bond type are both reported and (b) single bonds are followed by double bonds.

and this does not change much on creation of the hydrogen bond. The positive and negative values for DTC−MSA show the Ph−N−Ph backbone is normalizing; the dihedral split seen earlier is somewhat reduced on dimerization, though the two interplanar angles are still not the same. Overall, the reduction or rearrangement of the dihedral angles once again suggests a significant change in the electronic nature of the aniline backbone.

(b) Energetics (Table 1). The hydrogen bond strength, E_{HB}, for the reaction between the donor, N−H, and acceptor, O−S, was estimated from the total energy, E_{TOT}, of the monomers and the dimer using the following equation:

$$E_{HB} = E_{TOT}(\text{N−H}\cdots\text{O−S}) - [E_{TOT}(\text{N−H}) + E_{TOT}(\text{O−S})]$$

The resulting energy was adjusted for BSSE to correct for "borrowing" of basis functions within the dimer, and a ZPE correction was applied to compare with standard reaction enthalpies. The resulting bond strengths are shown in Table 1, and it can be seen the values vary from weak to strong over the eight dimers investigated. The variation occurs across both MSA and DMSO complexes, a useful sign that the use of DMSO is valid even though it is not as good a sulfonic acid model as MSA. In general, the alkyl-based models have weaker hydrogen bonds than their aryl equivalents, indicating the phenyl ring plays an important role in the strength of the bond. The two iminium cation models (MMA−DMSO and ICPA−DMSO) have very strong hydrogen bonds along with short bond lengths and high stretching frequencies. This is clearly due to the extra positive charge on both donors. In DTC−MSA, the best PANi/CSA model in this work, $E_{HB} \approx 39.5$kJ mol^{-1} per bond. This medium-strength hydrogen bond is therefore a fundamental part of the intermolecular structure of the PANi/CSA system.

(c) Natural Bond Orbital Analysis (Table 2). Geometry changes on hydrogen bonding between PANi and CSA models are of course only part of the story. The underlying electronic configuration of the hydrogen bonds and neighboring groups is crucial in understanding the full nature of the system. The changes in natural electronic population for each atom using the NBO method show a fairly consistent picture. N_C decreases while N_N increases, indicating there is charge transfer from phenyl to nitrogen occurring on dimerization. The electronegative nitrogen also receives electron density from its adjacent hydrogen (ΔN_H is negative), though some of this will go to form the hydrogen bond. The oxygen and sulfur populations change relatively little, but their contribution is more complicated and explained in the AIM section.

One of the advantages of the NBO method is the definition and analysis of distinct lone pair (LP) orbitals. This is particularly relevant to this work where the nitrogen LP has a crucial role in the transfer of electron density down the Ph−N−Ph backbone and hence the conductivity of the system. In the six unprotonated systems, the LP natural population, N_{LP}, decreases (along with the associated energetic destabilization) on creation of the hydrogen bond. This electron density is removed from the nitrogen atom (ΔN_N is positive), and any further delocalization is measured using the stabilization energy, $E^{(2)}$. In this case, $\Delta E^{(2)}_{LP(N)\rightarrow C=C^*}$, which measures the delocalization from the nitrogen LP into the C=C* antibonding orbitals on the adjacent phenyl rings, is consistently positive. So, on creation of the hydrogen bond, a significant amount of electron density is being delocalized from the nitrogen LP into the nitrogen at first and then into any adjacent phenyl rings. The measure of the change in delocalization *within* the ring, $\Delta E^{(2)}_{C=C\rightarrow C=C^*}$, is negligible and, in the best models, zero. This indicates that the changes in the electronic structure occur around the hydrogen bond system, (R)N−H···O−S and its associated lone pairs, as opposed to within the phenyl rings. Presumably the ability of the Ph−N−Ph backbone to conduct is controlled by how efficient the transfer of electron density across the nitrogen atom is, and these results suggest that hydrogen bonding to the nitrogen enhances this.

Last, $\sum E^{(2)}_{LP(O)\rightarrow N-H^*}$ measures the delocalization energy from the oxygen lone pair on the acceptor to the N−H* antibonding orbital on the donor. The near-linear correlation between this quantity and the hydrogen bond strength is shown in Figure 5.

(d) Atoms-In−Molecules Analysis (Table 3). The various charge flows on dimerization calculated using the AIM method (Table 3) show a picture similar to that seen in the NBO section. N_C and N_H decrease while N_N increases, consistent with the proposal that there is an increase in charge transfer from the phenyl rings to the central nitrogen on creation of the hydrogen bond. However, the charge flow on the oxygen and sulfur atoms, which was almost negligible in the NBO analysis, is more significant here. ΔN_O is negative, partly due to the creation of the adjacent hydrogen bond, but also ΔN_S is positive. The definition of the atom in AIM is the reason for the difference between the two analyses. In NBO the atomic population is defined as the total population of the constituent natural atomic orbitals for that atom. By contrast, in AIM each atom is defined by a boundary condition where $\nabla\rho = 0$. This atomic basin incorporates any lone pairs associated with the atom, and hence, AIM atomic populations will include LP contributions. In this case, N_O is decreased on dimerization because the oxygen LPs delocalize into an N−H* antibonding orbital as shown in the NBO section.

The results of a topological analysis of the charge distribution around the eight hydrogen bonds are presented in Table 3. The

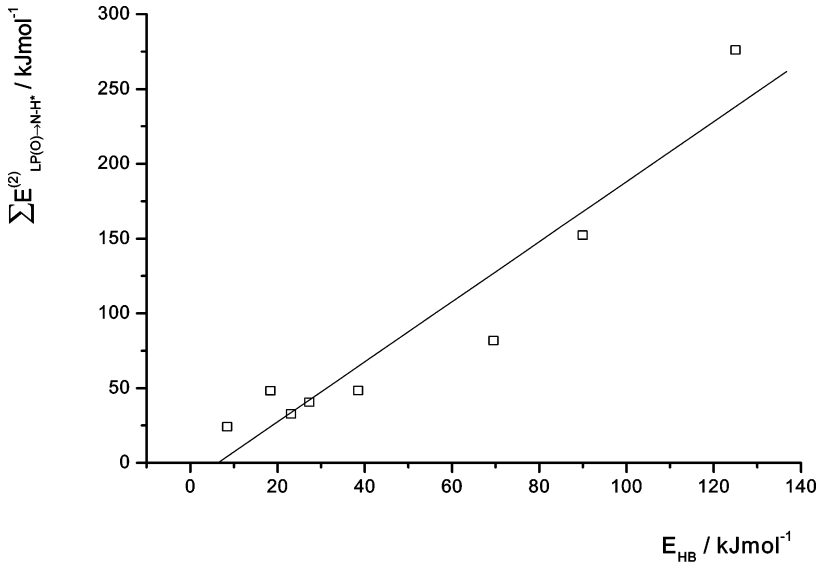

Figure 5. Graph showing the correlation between the delocalization energy for the oxygen lone pair to N−H* antibonding orbital process ($\sum E^{(2)}_{LP(O)\rightarrow N-H^*}$) and the hydrogen bond strength (E_{HB}).

TABLE 3: B3LYP/6-311++G(2d,2p)//BLYP/6-31G(d,p)[a]

dimer	ΔN_C	ΔN_N	ΔN_H	ΔN_O	ΔN_S	ϵ(HB)	ρ_c(HB)	$\Delta\epsilon$(N−C)	$\Delta\rho_c$(N−C)	$\Delta\epsilon$(N−H)	$\Delta\rho_c$(N−H)	$\Delta\epsilon$(O−S)
DMA−MSA	−0.010	+0.042	−0.107	−0.088	+0.264	0.000	0.0252	+0.003	+0.0052	−0.012	−0.0078	−0.005
DMA−DMSO	−0.008	+0.028	−0.065	−0.063	+0.057	0.010	0.0197	+0.006	+0.0027	−0.003	−0.0022	−0.001
MMA−DMSO	−0.016, +0.010	+0.051	−0.099	−0.050	+0.162	0.029	0.0816	−0.006, +0.035	+0.0121, +0.0055	−0.003	−0.0737	+0.018
DAZO−MSA	−0.027	+0.067	−0.116	−0.093	+0.271	0.009	0.0235	+0.013	+0.0096	−0.002	−0.0080	−0.001
DPA−MSA	−0.015	+0.038	−0.113	−0.089	+0.280	0.032	0.0355	+0.008	+0.0085	−0.016	−0.0226	−0.003
DPA−DMSO	−0.006	+0.030	−0.072	−0.052	+0.095	0.021	0.0261	+0.004	+0.0046	−0.010	−0.0101	+0.009
ICPA−DMSO	−0.009, −0.011	+0.046	−0.100	−0.032	+0.138	0.036	0.0519	−0.006, +0.013	+0.0073, +0.0063	−0.009	−0.0369	+0.018
DTC−MSA	−0.009, −0.010	+0.024, +0.026	−0.091, −0.092	−0.091, −0.096	+0.287	0.047, 0.011	0.0259, 0.0259	+0.005, +0.006	+0.0043, +0.0056	−0.013, −0.013	−0.0153, −0.0153	−0.007, −0.008

[a] Bond critical point ellipticity ϵ and bond critical point density ρ_c in au. The table is divided into alkyl-based models followed by aryl-based models. Δ values refer to the change in property on complexation. Where appropriate (a) two instances of one bond type are both reported and (b) single bonds are followed by double bonds.

absolute value of the ellipticity, ϵ, at the bond critical points in most cases is near zero, and in particular, ϵ(HB) $\approx$ 0. This indicates these bonds are single σ-type bonds and circular in cross-section. The exceptions to this (not shown) are the phenyl C−C bonds, where $\epsilon \approx 0.2$, indicating delocalized π-type bonds, and the Ph−N bonds, where $\epsilon \approx 0.1$. This result confirms that the Ph−N bonds are intermediate between single and double, and is another indication that the π-system on the phenyl rings delocalizes across the central nitrogen atom. The values of ρ_c (not shown) indicate that all the bonds in the compounds studied are covalent as expected, the only exception being for the hydrogen bonds where ρ_c(HB) is small, typical of a weaker interaction. Comparison of ρ_c in the amines studied here with equivalent alkyl- and arylphosphines[18] reveals that the corresponding bonds in phosphines have lower ρ_c values, indicating they are more ionic in nature than those studied here.

The changes in ϵ and ρ_c upon complexation reported in the remainder of Table 3 are mostly very small and less informative. Generally, in N−H and S−O bonds ϵ and ρ_c are reduced, and in N−C bonds ϵ and ρ_c are increased. An increasing ellipticity of the N−C bond would generally point to an increase in its π-character. However, the effect is so small, even in DTC−MSA, and the same effect is observed in both the alkyl and aryl complexes that no real significance can be applied to this result.

4. Conclusions

After a thorough investigation into the structural and electronic changes that occur on complexation between polyaniline and sulfonic acid models, a number of conclusions can be drawn. The most important of these is that the creation of a hydrogen bond between the amine and sulfonic acid groups acts to increase the ability of the phenyl−nitrogen−phenyl backbone to transfer electron density. The consequences of applying this result to the macromolecular system are clear. The capacity of the polyaniline backbone to conduct electricity can only be enhanced by the act of hydrogen bonding a sulfonic acid to it.

In addition, the mechanism of the enhanced transfer has been shown to be most likely via an increase in the amount of π-electrons in the phenyl−nitrogen bond. The influence the various lone pairs play in the system cannot be underestimated, and their interactions within the system have been examined.

Acknowledgment. We thank the EPSRC and DERA for funding this project. J.P.F. also thanks Jamie Platts (University of Cardiff) and Doug Fox (Gaussian Inc.) for several useful suggestions.

References and Notes

(1) *Science and Applications of Conducting Polymers*; Hilger: Bristol, U.K., 1991.

(2) Pouget, J. P.; Józefowicz, M. E.; Epstein, A. J.; Tang, X.; Macdiarmid, A. G. *Macromolecules* **1991**, *24*, 779.

(3) Epstein, A. J.; Macdiarmid, A. G. *Science and Applications of Conducting Polymers*; Hilger: Bristol, U.K., 1991; p 141. (b) Kenwright, A.; Feast, W. J.; Adams, P.; Milton, A.; Monkman, A. P.; Say, B. *Polymer* **1992**, *33*, 4292. (c) Adams, P.; Apperley, D. C.; Monkman, A. P. *Polymer* **1993**, *34*, 328. (d) Pomfret, S. J.; Adams, P. N.; Comfort, N. P.; Monkman, A. P. *Adv. Mater.* **1998**, *10*, 1351.

(4) Cao, Y.; Smith, P.; Heeger, A. J. US Patent No. 5232631, 1993. (b) Cao, Y.; Smith, P.; Heeger, A. J. *Synth. Met.* **1992**, *48*, 91.

(5) Ikkala, O. T.; Pietilä, L-O.; Ahjopalo, L.; Österholm, H.; Passiniemi, P. J. *J. Chem. Phys.* **1995**, *103*, *22*, 9855.

(6) Vaschetto, M. E.; Retamal, B. A.; Contreras, M. L.; Zagal, J. H. *Struct. Chem.* **1997**, *8*, 2, 121.

(7) Li, Z.-R.; Yang, M.-H.; Yang, J.; Ti, A.−M.; Yan, G.-S. *Acta Chim. Sin.* **1996**, *54*, 961.

(8) Shacklette, L. W. *Synth. Met.* **1994**, *65*, 123.

(9) Bahçeci, S.; Toppare, L.; Yurtsever, E. *Synth. Met.* **1994**, *68*, 57.

(10) Bahçeci, S.; Toppare, L.; Yurtsever, E. *Synth. Met.* **1996**, *81*, 5.

(11) de Oliveira, Z. T., Jr.; dos Santos, M. C. *Chem. Phys.* **2000**, *260*, 95.

(12) de Oliveira, Z. T., Jr.; dos Santos, M. C. *Solid State Commun.* **2000**, *114*, 49. (b) Stafström, S. *Synth. Met.* **1991**, *41*−*43*, 3697.

(13) Sein, L. T., Jr.; Wei, Y.; Jansen, S. A. *Comput. Theor. Polym. Sci.* **2001**, *11*, 83.

(14) Boyle, A. *J. Mol. Struct.: THEOCHEM* **1999**, *469*, 15.

(15) Baird, N. C.; Wang, H. Z. *Chem. Phys. Lett.* **1993**, *202*, 501.

(16) Jansen, S. A.; Duong, T.; Major, A.; Wei, Y.; Sein, L. T., Jr. *Synth. Met.* **1999**, *105*, 107. (b) Sein, L. T., Jr.; Duong, T.; Wei, Y.; Jansen, S. A. *Synth. Met.* **2000**, *113*, 145. (c) Sein, L. T., Jr.; Duong, T.; Major, A.; Kolla, S.; Wei, Y.; Jansen, S. A. *J. Mol. Struct.: THEOCHEM* **2000**, *498*, 37. (d) Sein, L. T., Jr.; Wei, Y.; Jansen, S. A. *Synth. Met.* **2000**, *108*, 101.

(17) Wang, Y.; Saebo, S.; Pittman, C. U., Jr. *J. Mol. Struct.: THEOCHEM* **1993**, *281*, 91.

(18) Howard, S. T.; Foreman, J. P.; Edwards, P. G. *Inorg. Chem.* **1996**, *35*, 5805.

(19) Howard, S. T.; Foreman, J. P.; Edwards, P. G. *Chem. Phys. Lett.* **1997**, *264*, 454. (b) Howard, S. T.; Foreman, J. P.; Edwards, P. G. *Can. J. Chem.* **1997**, *75*, 60.

(20) Cavazzoni, C.; Colle, R.; Farchioni, R.; Grosso, G. *Phys. Rev. B* **2002**, *66*, 165110. (b) Lim, S. L.; Tan, K. L.; Kang, E. T.; Chin, W. S. *J. Chem. Phys.* **2000**, *112*, 10648.

(21) See, for example: (a) Ha, T. K.; Suleimenova, O. M.; Han, M. J. *J. Mol. Struct.: THEOCHEM* **2001**, *574*, 75. (b) Lukin, O.; Leszczynski, J. *J. Phys. Chem. A* **2002**, *106*, 6775.

(22) Foreman, J. P.; Monkman, A. P. Manuscript in preparation.

(23) Becke, A. D. *J. Chem. Phys.* **1993**, *98*, 5648.

(24) Hariharan, P. C.; Pople, J. A. *Theor. Chim. Acta* **1973**, *14*, 213.

(25) Boys, S. F.; Bernadi, F. *Mol. Phys.* **1970**, *19*, 553.

(26) Krishnan, R.; Binkley, J. S.; Seeger, R.; Pople, J. A. *J. Chem. Phys.* **1980**, *72*, 650.

(27) Gaussian 98, Revision A.11.3: Frisch, M. J.; Trucks, G. W.; Schlegel, H. B.; Scuseria, G. E.; Robb, M. A.; Cheeseman, J. R.; Zakrzewski, V. G.; Montgomery, J. A., Jr.; Stratmann, R. E.; Burant, J. C.; Dapprich, S.; Millam, J. M.; Daniels, A. D.; Kudin, K. N.; Strain, M. C.; Farkas, O.; Tomasi, J.; Barone, V.; Cossi, M.; Cammi, R.; Mennucci, B.; Pomelli, C.; Adamo, C.; Clifford, S.; Ochterski, J.; Petersson, G. A.; Ayala, P. Y.; Cui, Q.; Morokuma, K.; Rega, N.; Salvador, P.; Dannenberg, J. J.; Malick, D. K.; Rabuck, A. D.; Raghavachari, K.; Foresman, J. B.; Cioslowski, J.; Ortiz, J. V.; Baboul, A. G.; Stefanov, B. B.; Liu, G.; Liashenko, A.; Piskorz, P.; Komaromi, I.; Gomperts, R.; Martin, R. L.; Fox, D. J.; Keith, T.; Al-Laham, M. A.; Peng, C. Y.; Nanayakkara, A.; Challacombe, M.; Gill, P. M. W.; Johnson, B.; Chen, W.; Wong, M. W.; Andres, J. L.; Gonzalez, C.; Head-Gordon, M.; Replogle, E. S.; Pople, J. A., Gaussian, Inc., Pittsburgh, PA, 2002.

(28) Weinhold, F. Natural Bond Orbital Methods. In *Encyclopedia of Computational Chemistry*; Schleyer, P. v. R., Allinger, N. L., Clark, T., Gasteiger, J., Kollman, P. A., Schaefer, H. F., III, Schreiner, P. R., Eds.; John Wiley & Sons: Chichester, U.K., 1998; Vol. 3, p 1792. (b) Reed, A. E.; Weinstock, R. B.; Weinhold, F. *J. Chem. Phys.* **1985**, *83*, 735.

(29) NBO 5.0: Glendening, E. D.; Badenhoop, J. K.; Reed, A. E.; Carpenter, J. E.; Bohmann, J. A.; Morales, C. M.; Weinhold, F., Theoretical Chemistry Institute, University of Wisconsin, Madison, WI, 2001; http://www.chem.wisc.edu/~nbo5.

(30) Bader, R. F. W. *Atoms in Molecules: A Quantum Theory*; Oxford University Press: Oxford, U.K., 1990.

(31) Biegler-König, F. W.; Bader, R. F. W.; Tang, T.-H. *J. Comput. Chem.* **1982**, *3*, 317. These programs are available free of charge as either source code (AIMPAC) or precompiled (AIM2000) binaries from http://www.chemistry.mcmaster.ca/aimpac/ or http://gauss.fh-bielefeld.de/aim2000/, respectively.

(32) Hehre, W. J.; Radom, L.; Schleyer, P. v. R.; Pople, J. A. *Ab Initio Molecular Orbital Theory*: John Wiley & Sons: New York, 1986.